
ENS-10: A Dataset For Post-Processing Ensemble Weather Forecasts

Saleh Ashkboos
ETH Zürich
saleh.ashkboos@inf.ethz.ch

Langwen Huang
ETH Zürich
langwen.huang@inf.ethz.ch

Nikoli Dryden
ETH Zürich
ndryden@ethz.ch

Tal Ben-Nun
ETH Zürich
talbn@inf.ethz.ch

Peter Dueben
ECMWF
peter.dueben@ecmwf.int

Lukas Gianinazzi
ETH Zürich
glukas@ethz.ch

Luca Kummer
ETH Zürich
lkummer@student.ethz.ch

Torsten Hoefler
ETH Zürich
htor@inf.ethz.ch

Abstract

Post-processing ensemble prediction systems can improve weather forecasting, especially for extreme event prediction. In recent years, different machine learning models have been developed to improve the quality of the post-processing step. However, these models heavily rely on the data and generating such ensemble members requires multiple runs of numerical weather prediction models, at high computational cost. This paper introduces the ENS-10 dataset, consisting of ten ensemble members spread over 20 years (1998–2017). The ensemble members are generated by perturbing numerical weather simulations to capture the chaotic behavior of the Earth. To represent the three-dimensional state of the atmosphere, ENS-10 provides the most relevant atmospheric variables in 11 distinct pressure levels as well as the surface at 0.5° resolution. The dataset targets the prediction correction task at 48-hour lead time, which is essentially improving the forecast quality by removing the biases of the ensemble members. To this end, ENS-10 provides the weather variables for forecast lead times $T=0, 24,$ and 48 hours (two data points per week). We provide a set of baselines for this task on ENS-10 and compare their performance in correcting the prediction of different weather variables. We also assess our baselines for predicting extreme events using our dataset. The ENS-10 dataset is available under the Creative Commons Attribution 4.0 International (CC BY 4.0) licence.

1 Introduction

Weather forecasting is among the most critical scientific applications with a significant influence on society and the economy [16]. Predicting the trajectory of a hurricane or tropical cyclone can save lives and billions of dollars in damages by allowing adequate mitigation efforts [20]. Moreover, weather forecasts can improve agricultural yield [40, 41] and guide decisions in aviation [11] and maritime ship transport [22]. However, predicting the weather and extreme events are among the most complex tasks due to their chaotic behavior [25], and there has been an enormous amount of effort to tackle this problem in recent years [1, 4, 18, 36].

In the last decades, predicting weather variables (like temperature or precipitation) has been done by solving complex partial differential equations (PDEs) [19, 21]. To this end, Numerical Weather

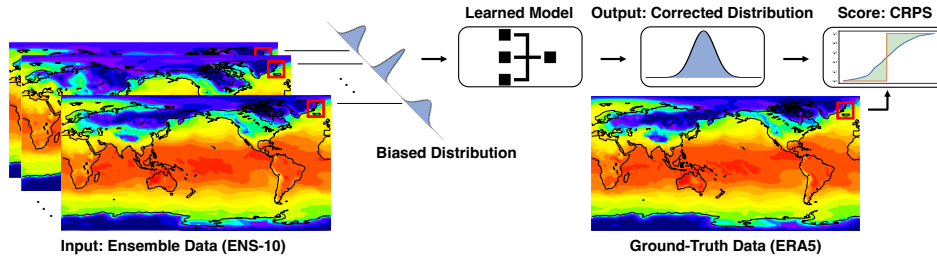


Figure 1: The post-processing pipeline feeds the ENS10 ensemble, representing a biased distribution, to the deep learning model, which predicts a *corrected* distribution. This corrected distribution is scored against ERA5 ground truth data with the Continuous Ranked Probability Score (CRPS).

Prediction (NWP) models start from an initial weather condition and output the new conditions by solving a set of PDEs. However, as a single simulation cannot represent the chaotic behavior of the environment [25], ensemble weather prediction is introduced to quantify such uncertainty. In such methods, the initial conditions of the environment are perturbed multiple times, and the NWP models operate on these ensemble members to generate a set of forecasts. However, running the numerical models incurs high computational costs. In addition, ensemble weather prediction suffers from systematic errors, known as biases, which are introduced during either the generation of initial conditions or the simulation itself [35].

Ensemble post-processing approaches have been proposed to improve forecast skill by correcting the output distribution of the ensemble weather prediction models, known as *prediction correction*. The goal of prediction correction is to remove the biases of NWP outputs. In recent years, deep learning models [2, 7, 10, 17, 26, 29] have shown promising results over the well-known statistical methods [36] (e.g., EMOS [9], Bayesian Moving Averages [27]) in the prediction correction task. Figure 1 summarizes the key steps of a deep learning-based post-processing pipeline. However, the performance of these models heavily depends on the available training data and the field suffers from the lack of a unified and standard ensemble dataset, as constructing an ensemble requires running multiple numerical models at a high computational cost. This makes training and comparing the performance of machine learning models for prediction correction challenging.

To address this challenge, we introduce the ENS-10 dataset, a collection of 10 perturbed ensemble members over 20 years (1998–2017) for medium-range ensemble forecasts (lead time 48 hours). To represent the state of the atmosphere, we provide the most relevant atmospheric fields at 11 different pressure levels as well as on the surface on a structured longitude/latitude grid with a 0.5° resolution. We first define the prediction correction task and propose two metrics of skill: Continuous Ranked Probability Score (CRPS) and the novel Extreme Event Weighted Continuous Ranked Probability Score (EECRPS). The weighted score gives importance to points where the ensemble members deviate from the climatology, rewarding skill on challenging, potentially unusual weather phenomena. As a benchmark, we provide a set of baselines to apply unsupervised, statistical, and DNN-based supervised learning solutions (with different architectures) to the prediction correction task. Finally, we provide a set of Python interfaces to download, train, and compare different models.

1.1 Related Work

Data-driven weather forecasting focuses on training a learned model to predict weather variables. Such methods start from a deterministic atmospheric condition and generate the next state using a neural network. In recent years, different architectures like fully connected networks [5], convolutional networks [5, 30, 33, 34], LSTMs [39], and transformers [24] have been applied to tackle this problem.

As data-driven forecasting approaches heavily depend on the data, they usually use *reanalysis*, namely reproducing historical weather data consistently with an existing NWP model, as ground truth. To this end, different datasets such as ERA5 [13] and CFSR [32] have been developed and used as the input of the neural networks. Recently, WeatherBench [28] provided a set of benchmarks and metrics on a subset of the ERA5 dataset to accelerate data-driven weather forecasting research.

In contrast to deterministic data-driven forecasting, we focus on ensemble processing methods [36]. These methods operate on a set of ensembles, each generated by running a NWP simulation on perturbed initial atmospheric conditions. The goal is to correct the prediction by mitigating the biases of the ensemble outputs, known as ensemble post-processing. Statistical methods such as ensemble model output statistics (EMOS) [9] and Bayesian moving averages (BMA) [27] have been proposed to correct such biases in last decades.

Recent work has developed deep learning models for ensemble post-processing. To this end, different architectures, e.g., shallow fully connected networks [7, 29], LeNet-style convolutional networks [17], and U-Net-style networks [10] have been proposed. However, as each work utilizes its own dataset and loss metrics, it is imperative to standardize data and benchmarking of NWP post-processing. In this work, we propose ENS-10 to fill this gap and provide an easy-to-use interface for using it.

2 ENS-10 Dataset

2.1 Data Collection

Global weather predictions are performed operationally in certain time intervals and often use ensembles of simulations for uncertainty quantification — for example, a 50-member ensemble twice a day at the European Centre for Medium-range Weather Forecasts (ECMWF).

To derive a long-term training dataset that provides consistent quality for ensemble simulations, we use reforecasts [12], which are ensemble weather predictions that run routinely at ECMWF to simulate the weather over the past 20 years. The resulting dataset is used to provide an estimate of the climate for each date to measure the *skill* of the forecast system [37, 38]. The reforecasts that were used for this dataset were generated by a model with 91 vertical levels using the Integrated Forecast System of ECMWF [6]. Reforecasts are generated for the time period from January 1998 to December 2017 and two simulations are started per week. The model uses a spectral representation of the model fields and a cubic octahedral reduced Gaussian grid is used to represent fields in grid-point space with a grid-spacing of approximately 36 km. As machine learning solutions often make use of convolutions in horizontal directions, we map the model fields and the ERA5 dataset onto a structured longitude/latitude grid with a 0.5° resolution. The dataset is approximately 3 TB in size.

2.2 Dataset Features

The weather models typically use approximately 10 prognostic variables per grid point. However, not all variables will be useful to perform post-processing for a selection of model fields that are of interest. We therefore aim to reduce the input fields to those fields that hold the most significant amount of information about the three-dimensional state of the atmosphere.

ENS-10 consists of the atmospheric fields that appear most relevant in this context (see Table 1). Some of the fields are available at the surface (e.g., the wind at 10 meter height in the zonal and meridional directions, U10m and V10m, or temperature at 2 meters above ground, T2m). Other fields are integrated quantities over the vertical column of the atmospheric model resulting in two-dimensional horizontal fields that are classified as surface fields (e.g., total column water, TCW). Finally, some of the fields are diagnosed at pressure levels along the vertical direction of the atmosphere. Our dataset provides some of the model fields at 11 distinct pressure levels between 10 and 1000 hPa, to describe the state of the atmosphere from the surface to the stratosphere. The dataset contains the fields at lead times of 0, 24, and 48 hours starting from two dates per week over a span of 20 years.

2.2.1 Surface Level Features

The following variables are provided at surface level¹.

Sea Surface Temperature (SST) is the temperature of the sea in units of kelvin.

Total Column Water (TCW) is the sum of water vapour, liquid water, cloud ice, rain, and snow in a column extending from the surface of the Earth to the top of the atmosphere. It is saved in units of kilogram per square meter.

¹Full definitions at <https://apps.ecmwf.int/codes/grib/param-db/>

Table 1: Parameters of ENS-10. The dataset contains each parameter for 10 different ensemble members on resolution 0.5° latitude/longitude grids at 0, 24, and 48 hour forecast lead times.

Name	Abbreviation	Pressure Level	Unit	Range
Sea surface temperature	SST		K	[261.2, 308.7]
Total Column Water	TCW		kg/m ²	[0, 133.4]
Total column water vapour	TCWV		kg/m ²	[0, 94.29]
Convective precipitation	CP		m	[0, 0.8552]
Mean sea level pressure	MSL		Pa	[90723, 107485]
Total cloud cover	TCC	Surface	(0–1)	[0, 1]
10 m U wind component	U10m		m/s	[-42.18, 41.18]
10 m V wind component	V10m		m/s	[-42.93, 46.21]
2 m temperature	T2m		K	[190.8, 324.0]
Total precipitation	TP		m	[0, 1.158]
Skin temperature at the surface	SKT		K	[188.6, 333.7]
U wind component	U		m/s	[-133.49, 151.48]
V wind component	V		m/s	[-133.64, 134.08]
Geopotential	Z	10/50/100/200/300/400/	m ² /s ²	[-7659.2, 316357]
Temperature	T	500/700/850/925/1000 hPa	K	[164.99, 329.14]
Specific humidity	Q		kg kg ⁻¹	[-0.0100, 0.0400]
Vertical velocity	W		Pa/s	[-19.282, 16.351]
Divergence	D		/s	[-0.0017, 0.0015]

Total Column Water Vapour (TCWV) is the amount of water vapour in a column extending from the surface of the Earth to the top of the atmosphere. Like TCW, this field is saved in units of kilogram per square meter.

Convective Precipitation (CP) is the accumulated liquid and frozen water, comprising rain and snow, that falls to the Earth’s surface, which is generated by the convection scheme in units of meters.

Mean Sea Level pressure (MSL) is the pressure (force per unit area) of the atmosphere adjusted to the height of mean sea level in units of pascals.

Total Cloud Cover (TCC) is the proportion of a grid column covered by cloud calculated as a single level field from the clouds occurring at different model levels through the atmosphere.

10m U wind component (U10m) is the eastward component of the wind 10 meters above the ground in units of meters per second.

10m V wind component (V10m) is the northward component of the wind 10 meters above the ground in units of meters per second.

2m Temperature (T2m) is the temperature of air at 2 m above the surface of land, sea or in-land waters calculated by interpolating between the lowest model level and the Earth’s surface, taking account of the atmospheric conditions. The field is saved in units of kelvin.

Total Precipitation (TP) is the accumulated liquid and frozen water, comprising rain and snow, that falls to the Earth’s surface. It is the sum of large-scale precipitation and convective precipitation and saved in units of meters.

Skin temperature at the surface (SKT) indicates the temperature of the uppermost surface layer, which has no heat capacity and so can respond instantaneously to changes in surface fluxes in kelvin.

2.2.2 Volumetric Features

The dataset provides the following seven fields at 11 distinct pressure levels between 10 and 1000 hPa, to describe the state of the atmosphere from the surface to the stratosphere.

U wind component (U) is the eastward component of the wind at each pressure level. It is the horizontal speed of air moving towards the east, in units of meters per second. A negative sign thus indicates air movement towards the west.

V wind component (V) is the northward component of the wind at each pressure level. It is the horizontal speed of air moving towards the north, in units of meters per second. A negative sign thus indicates air movement towards the south.

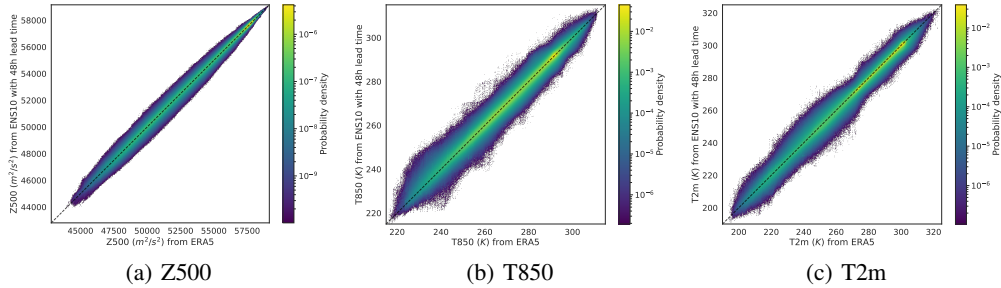


Figure 2: A scatterplot of the raw ENS-10 ensemble forecast against the ERA5 reanalysis reveals varying levels of uncertainty for different target variables. Moreover, certain ranges of values are better characterized by the raw forecast than others. Post-processing corrects the raw ensemble distribution to remove biases and improve the forecast skill.

Geopotential (Z) is the gravitational potential energy of a unit mass, at a particular location, relative to mean sea level at each pressure level. It is also the amount of work that would have to be done, against the force of gravity, to lift a unit mass to that location from mean sea level. The variable is saved in units of m^2/s^2 .

Temperature (T) shows the temperature at each pressure level. The field is saved in units of kelvin.

Specific humidity (Q) is the mass of water vapour per kilogram of moist air at each pressure level. The total mass of moist air is the sum of the dry air, water vapour, cloud liquid, cloud ice, rain and falling snow. The field is saved in units of kilograms per kilogram.

Vertical Velocity (W) is the air speed in the upward or downward direction at each pressure level in units of pascals per second.

Divergence (D) is the rate of spreading the air from a point per square meter at each pressure level in the inverse second. The negative values shows that the air is concentrating.

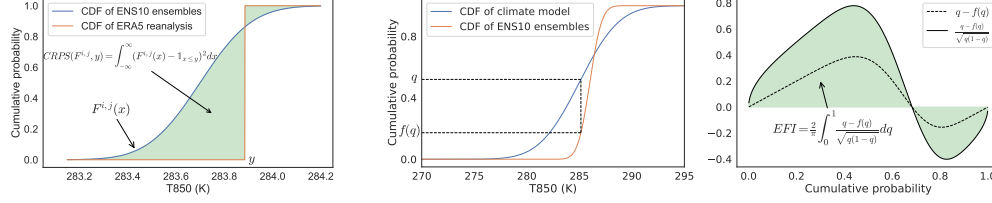
3 Task

The ultimate goal of ensemble processing is to correct the prediction by post-processing the ensemble members (see Figure 2). In this section, we define the prediction correction task for different variables using the ENS-10 dataset. We provide different evaluation metrics to assess the quality of a given solution for this task on weather and extreme event forecasting. We also study the role of varying number of ensemble members on the quality of a solution in our task.

3.1 Prediction Correction

For a given time T , the input is a set of ensemble members $E = \{E_{k,T}\}_{k \in [1,10]}$. Each ensemble member $E_{k,T}$ contains all surface and volumetric features at time steps T , $T + 24$ h, and $T + 48$ h. For a given target variable at a specific pressure level (or at the surface), the task is to predict a *corrected* cumulative distribution function (CDF) $F^{i,j}$ for that variable at time $T + 48$ h at each grid point (i, j) (at the specified pressure level). Usually, this is achieved by estimating the parameters of a probability distribution. Many previous works [10, 26, 29] assume a Gaussian distribution at each grid point and estimate the means and standard deviations. We follow this approach for our baselines. However, in general, any distribution or distribution representation may be assumed.

In particular, we consider three target variables: **2 m temperature (T2m)**, **temperature at 850 hPa (T850)**, and **geopotential at 500 hPa (Z500)**. The years 1998–2015 are used as the training set and 2016–2017 as the test set. We use ERA5 as ground truth data for the exact weather at prediction time.



(a) CRPS is calculated by integrating the square of the difference between the ensemble CDF and the reanalysis CDF (green area). (b) **Left:** $f(q)$ is the cumulative probability of the ensemble values that is smaller than the q -quantile of the climate model. **Right:** EFI integrates the difference between the model climate and the ensemble forecast, but gives more weight to the extreme values.

Figure 3: Visualization of CRPS and EFI for predicting the temperature at 850 hPa.

3.2 Evaluation Metrics

To evaluate a potential solution for our task, we use two different metrics as scores for prediction skill. **CRPS** is used for scoring predictions in general. We also define a novel metric, called **ECCRPS**, which assesses the correction’s improvement in skill for extreme event prediction.

Continuous Ranked Probability Score (CRPS). The corrected CDF F is evaluated against the ERA5 ground-truth with CRPS [43]. CRPS generalizes the mean absolute error for the case where forecasts are probabilistic. Let $\mathbb{1}_{x \leq y}$ be an indicator function that is 1 if $x \leq y$ and 0 otherwise. Formally, given the ground truth observation x at grid-point (i, j) , the CRPS for the corrected CDF F at point (i, j) is

$$\text{CRPS}(F^{i,j}, x) = \int_{-\infty}^{\infty} (F^{i,j}(y) - \mathbb{1}_{x \leq y})^2 dy, \quad (1)$$

where the integration is over the range of possible outcomes for the target variable (see Figure 3(a)). The CRPS assumes F has finite expectation. We report the mean CRPS over all grid points over the two test years, and for each day, we consider the variable at 00:00 UTC. The CRPS integral can often be solved in closed form using an identity by Baringhaus and Franz [3, 8].

Extreme Event Weighted Continuous Ranked Probability Score (ECCRPS). A crucial goal in correcting prediction biases is mitigating uncertainty during extreme weather events. In order to avoid muddling such events with forecast skill in the average case, we define a weighted version of CRPS that emphasizes such events.

A widely used metric that defines the irregularity of forecast field values is the extreme forecast index (EFI) [15, 44]. The EFI measures the deviation of the ensemble forecast relative to a probabilistic climate model (see Figure 3(b)). The EFI ranges between -1 and 1 , where large absolute values indicate a larger deviation from the meteorological record. Generally, values of magnitude between $0.5 - 0.8$ are considered *unusual* and values above 0.8 are considered *very unusual* and indicate that extreme weather is likely. Therefore, given the ground-truth observation y at grid-point (i, j) , we use the absolute value of EFI at that point to weight the CRPS as a secondary score:

$$\text{ECCRPS}(F^{i,j}, y) := |\text{EFI}_{(i,j)}| \times \text{CRPS}(F^{i,j}, y). \quad (2)$$

We report the mean ECCRPS over all grid points of the test years.

Given a grid-point (i, j) , for each date, the climate model is an empirical distribution function of all ensemble predictions in a window around that date over many years at (i, j) . That is, a sliding window is used to select the ensembles for each date.

We calculate the $\text{EFI}_{(i,j)}$ for all grid-points (i, j) over the ENS-10 test set with 0.05-quantiles. To this end, at a specific date, we first calculate the cumulative histogram of the 10 ensemble members of our dataset at that date. Note that we use the same lead time of 48 h for all ensemble forecasts. Then, we aggregate ensemble predictions in a window of 9 dates centered around the selected date over the past 18 years. Hence, a total of $18 \times 9 \times 10$ ensemble members represent the climate model for each date. We calculate their quantiles from probability 0 to 1 at an interval of 0.05 as a discrete representation

of the inverse of the cumulative distribution function. In the end, the $\text{EFI}_{(i,j)}$ is calculated as

$$\text{EFI}_{(i,j)} = \frac{2}{\pi} \sum_{q \in \mathcal{Q}} \frac{q - f_{(i,j)}(q)}{\sqrt{q(1-q)}} \Delta q, \quad (3)$$

where $\Delta q = 0.05$, $\mathcal{Q} = \{0, 0.05, 0.1, \dots, 0.95, 1\}$, $f_{(i,j)}(q)$ is calculated from the q -quantile value of our climate model subtracted from the cumulative histogram at the position of the q -quantile value.

4 Benchmarks and Results

In this section, we define several benchmarks for the prediction correction task over ENS-10. These benchmarks differ based on their approach (model), the number of used ensembles, and the way they use the dataset as an input. For each benchmark, we evaluate a set of baselines models. All benchmarks are implemented in PyTorch [23] and included in the ENS-10 repository.

4.1 Baseline Models

A plethora of models have been developed to tackle the ensemble post-processing task during the past decades [7, 9, 10, 27, 29]. Our goal is to train these models to minimize CRPS. However, in general, CRPS is not a differentiable metric. To overcome this issue, following previous work [10, 26, 29], we assume a Gaussian distribution on the target variable and learn the mean and standard deviation of this distribution. In this case, the CRPS from Eqn. (1) can be rewritten as

$$\sigma \left[\frac{1}{\sqrt{\pi}} - 2\psi \left(\frac{y - \mu}{\sigma} \right) - \frac{x - \mu}{\sigma} \left(2\phi \left(\frac{x - \mu}{\sigma} \right) - 1 \right) \right], \quad (4)$$

where μ and σ are the mean and standard deviation of the distribution, and ψ and ϕ are the probability density and cumulative density function of a standard Gaussian random variable, respectively [8].

In the simplest case, one can use the mean and standard deviation of the raw ensemble members as a predictor without performing any correction. However, to improve forecasting quality, the mean and standard deviation can be estimated using simple statistical approaches [9, 27] or deep learning models [7, 10, 29]. We define our baselines next.

The **Raw** baseline refers to using the raw ensemble mean and standard deviation for prediction. We apply this baseline for predicting all three variables in the prediction correction task. To this end, we calculate the CRPS using the mean and standard deviation of the ensembles on each grid point at T=48 h on our test set. We also calculate the EECRPS for T2m at T + 48 h on the test set.

Ensemble Model Output Statistics (EMOS) [9] is a statistical method based on a linear relation between the ensemble values and the corrected mean and variance.

For a given set of ensemble members $E = \{E_{i,T}\}_{i \in [1,m]}$, EMOS assumes a Gaussian distribution over the variable of interest $Y \sim \mathcal{N}(\mu, \sigma^2)$ on each point and computes the mean μ and standard deviation σ using $\mu = a + \sum_{i=1}^m b_i E_{i,T}$ and $\sigma = c + d\sigma_E^2$, where σ_E^2 is the variance of the ensemble variables in E . However, for predicting a target variable (such as Z500), EMOS uses only the input features for Z500 and does not exploit the inter-variable relations for prediction improvement.

A **Multi-layer perceptron (MLP)** is a series of fully-connected layers followed by a non-linear function. For our baseline, we use an MLP with one hidden layer, following Rasp and Lerch [29]. The network corrects the prediction point-wise by estimating the corrected mean and standard deviation of a corrected Gaussian random variable. For each point, we provide the mean and standard deviation of all variables in ENS-10 at lead time T=48 h in the same pressure level as the variable of interest. In addition, we provide the spatial information of that point (latitude and longitude) in our baselines using a 3-dimensional xyz coordinate on a unit sphere where $x = \cos(\psi) \sin(\phi)$, $y = \cos(\psi) \cos(\phi)$, $z = \sin(\psi)$ and ψ, ϕ are longitude and longitude.

The MLP outputs two values associated with the mean and the standard deviation of the variable of interest. As we normalize the input to the network, to get the correct mean and standard deviation of a given input, we multiply the first output value with the standard deviation of the ensemble member and add the ensemble mean at that point. Similarly, we get the corrected standard deviation by taking

the exponential of the second output value and multiplying it with the ensemble standard deviation. The baseline network has 25 and 17 input dimensions (two inputs for each variable in the ENS-10 dataset and three for XYZ coordinates) for the surface and volumetric features, respectively. We use a hidden layer with dimension 128 and ReLU as the activation function.

The **U-Net** architecture is widely used in image segmentation tasks [31] and other tasks such as pixel-wise regression [42]. Recently, a U-Net style network has been applied to correcting the biases of ensembles [10]. We use a U-Net network as our baseline to predict the corrected mean and standard deviation of the Gaussian target variables.

Following Grönquist et al. [10], we create a U-Net baseline with three levels, each containing a set of [convolution, batch normalization, ReLU] modules. The network operates on the whole grid with 22 and 14 input dimensions (two inputs for each variable in the ENS-10 dataset) for the surface and volumetric features, respectively. We use convolutions with 32, 64, and 128 output channels in our network’s first, second, and third levels, respectively.

Input data to the U-Net are normalized. The network outputs two grids for the mean and standard deviation of the variable of interest. Similar to the MLP, we scale and add the value of the first output channel with the standard deviation and mean of the ensemble members in each grid point. Also, we take the exponential of the second output channel of the network and multiply it with the ensemble standard deviation to get the corrected standard deviation.

4.2 Baseline Scores

We train the EMOS, MLP, and U-Net models using the Adam optimizer [14] with learning rate 10^{-5} . We do not use any scheduler for the learning rate during the training. The input data is split into mini-batches according to the time index: each sample inside a mini-batch contains a "slice" of data with the same time index but different latitude/longitude indices. We use a batch size of 8 samples for the U-Net model, and 1 for the MLP and EMOS models, as larger batch sizes yielded degraded performance. We train all models for 10 epochs on a single A100 GPU. Training the baseline models took 0.75, 0.25, and 1 hours for EMOS, MLP, and U-Net models, respectively.

The input data normalization for the MLP and U-Net models is performed according to the mean and standard deviation over all the time steps and ensemble members. Specifically, for each input variable at each latitude/longitude, the value is subtracted by the time-ensemble mean and divided by the standard deviation. In this way, any Gaussian distributed value over time and ensembles can be scaled to the Gaussian distribution with mean 0 and standard deviation 1. The normalization process is performed independently for different latitudes or longitudes to flatten the variance over different locations, following Grönquist et al. [10].

Following the original implementation of EMOS [9], the normalization of input data for the EMOS model linearly scales each variable to the range between 0 and 1 using minimum and maximum values over all the time steps, ensemble members, and grid points.

In addition to using the whole dataset (ten ensemble members), to show the importance of the number of ensemble members on the prediction correction task, we repeat all our experiments with the first five ensemble members (half of the dataset) from ENS-10.

To evaluate the ability of our baselines on extreme event forecasting, we calculate the EECRPS of the T2m variable using the extracted EFI from our dataset (see Section 3.2 for more details). We use the absolute value of EFI to weight the CRPS metric before averaging over the global data points in our test set. Table 2 shows the results of our benchmarks with CRPS and EECRPS metrics. We train each model using three different random seeds and report the mean and standard deviation.

5 Conclusion

We present a dataset and metrics for learning weather prediction bias correction. In particular, ten high-resolution ensemble members were generated for 20 years of weather forecasts. To represent the atmospheric environment of the earth, the dataset consists of the 11 most relevant surface variables as well as 7 variables at 11 distinct pressure levels in 0.5° resolution. To measure prediction correction quality, we benchmark learned models using a widely-used score (CRPS) and a novel scoring function that prioritizes extreme weather events (EECRPS). As a baseline, we evaluate a set of statistical and

Table 2: Global mean CRPS and EECRPS on the test set (2016–2017) for our baseline models with five (5-ENS) or ten (10-ENS) ensemble members.

Metric	Model	Z500		T850		T2m	
		5-ENS	10-ENS	5-ENS	10-ENS	5-ENS	10-ENS
CRPS	Raw	81.03	78.24	0.748	0.719	0.758	0.733
	EMOS	79.08 \pm 0.739	81.74 \pm 6.131	0.725 \pm 0.002	0.756 \pm 0.052	0.718 \pm 0.003	0.749 \pm 0.054
	MLP	75.84 \pm 0.016	74.63 \pm 0.029	0.701 \pm 2e $-$ 4	0.684 \pm 4e $-$ 4	0.684 \pm 6e $-$ 4	0.672 \pm 5e $-$ 4
	U-Net	76.66 \pm 0.470	76.25 \pm 0.106	0.687 \pm 0.003	0.669 \pm 0.009	0.659 \pm 0.005	0.644 \pm 0.006
EECRPS	Raw	29.8	28.78	0.256	0.246	0.258	0.25
	EMOS	29.10 \pm 0.187	30.13 \pm 2.166	0.248 \pm 3e $-$ 4	0.259 \pm 0.018	0.245 \pm 0.001	0.255 \pm 0.018
	MLP	27.86 \pm 0.006	27.41 \pm 0.010	0.240 \pm 1e $-$ 4	0.234 \pm 2e $-$ 4	0.233 \pm 2e $-$ 4	0.229 \pm 2e $-$ 4
	U-Net	27.98 \pm 0.240	27.61 \pm 0.490	0.235 \pm 0.003	0.230 \pm 0.002	0.223 \pm 5e $-$ 4	0.219 \pm 0.001

machine learning models that are used by the weather and climate community on the dataset. By generating a high-resolution dataset of perturbed ensemble member simulations, ENS-10 enables data-driven global scale uncertainty quantification and bias correction, aiding in accurate pinpointing of extreme weather events. However, we caution that ENS-10 is not suitable on its own for tasks such as weather *prediction*; and further that its performance evaluation is necessarily predicated on the quality of the ERA5 reanalysis dataset we use as ground truth.

The ENS-10 dataset can be downloaded directly² or through a downloader Python script. Examining the raw data, preprocessing, normalization, and training are all provided through a set of Python APIs³, examples written in PyTorch, and Jupyter notebooks⁴.

Acknowledgements

This project received EuroHPC-JU funding under grant MAELSTROM, No. 955513. N.D. is supported by the ETH Postdoctoral Fellowship. T.B.N. is supported by the Swiss National Science Foundation (Ambizione Project #185778). We thank the Swiss National Supercomputing Center (CSCS) for providing computing resources.

References

- [1] Richard B Alley, Kerry A Emanuel, and Fuqing Zhang. Advances in weather prediction. *Science*, 363(6425):342–344, 2019.
- [2] Sándor Baran and Ágnes Baran. Calibration of wind speed ensemble forecasts for power generation. *arXiv preprint arXiv:2104.14910*, 2021.
- [3] L. Baringhaus and C. Franz. On a new multivariate two-sample test. *Journal of Multivariate Analysis*, 88(1):190–206, 2004.
- [4] Peter Bauer, Alan Thorpe, and Gilbert Brunet. The quiet revolution of numerical weather prediction. *Nature*, 525(7567):47–55, 2015.
- [5] Peter D Dueben and Peter Bauer. Challenges and design choices for global weather and climate models based on machine learning. *Geoscientific Model Development*, 11(10):3999–4009, 2018.
- [6] ECMWF. Modeling and prediction | ECMWF. <https://www.ecmwf.int/en/research/modelling-and-prediction>, 2022.

²https://storage.ecmwf.europeanweather.cloud/MAELSTROM_AP4/

³<https://github.com/spcl/ens10>

⁴<https://github.com/spcl/climetlab-maelstrom-ens10>

- [7] Mohammadvaghef Ghazvinian, Yu Zhang, Dong-Jun Seo, Minxue He, and Nelun Fernando. A novel hybrid artificial neural network-parametric scheme for postprocessing medium-range precipitation forecasts. *Advances in Water Resources*, 151:103907, 2021.
- [8] Tilmann Gneiting and Adrian E Raftery. Strictly proper scoring rules, prediction, and estimation. *Journal of the American Statistical Association*, 102(477):359–378, 2007.
- [9] Tilmann Gneiting, Adrian E Raftery, Anton H Westveld III, and Tom Goldman. Calibrated probabilistic forecasting using ensemble model output statistics and minimum crps estimation. *Monthly Weather Review*, 133(5):1098–1118, 2005.
- [10] Peter Grönquist, Chengyuan Yao, Tal Ben-Nun, Nikoli Dryden, Peter Dueben, Shigang Li, and Torsten Hoefler. Deep learning for post-processing ensemble weather forecasts. *Philosophical Transactions of the Royal Society A*, 379(2194):20200092, 2021.
- [11] Ismail Gultepe, R Sharman, Paul D Williams, Binbin Zhou, G Ellrod, P Minnis, S Trier, S Griffin, Seong Yum, B Gharabaghi, et al. A review of high impact weather for aviation meteorology. *Pure and applied geophysics*, 176(5):1869–1921, 2019.
- [12] Thomas M. Hamill, Jeffrey S. Whitaker, and Steven L. Mullen. Reforecasts: An important dataset for improving weather predictions. *Bulletin of the American Meteorological Society*, 87(1), 2006.
- [13] Hans Hersbach, Bill Bell, Paul Berrisford, Shoji Hirahara, András Horányi, Joaquín Muñoz-Sabater, Julien Nicolas, Carole Peubey, Raluca Radu, Dinand Schepers, et al. The era5 global reanalysis. *Quarterly Journal of the Royal Meteorological Society*, 146(730):1999–2049, 2020.
- [14] Diederik P Kingma and Jimmy Ba. Adam: A method for stochastic optimization. *arXiv preprint arXiv:1412.6980*, 2014.
- [15] Francois Lalaurette. Early detection of abnormal weather conditions using a probabilistic extreme forecast index. *Quarterly Journal of the Royal Meteorological Society: A journal of the atmospheric sciences, applied meteorology and physical oceanography*, 129(594):3037–3057, 2003.
- [16] Jeffrey K Lazo, Rebecca E Morss, and Julie L Demuth. 300 billion served: Sources, perceptions, uses, and values of weather forecasts. *Bulletin of the American Meteorological Society*, 90(6), 2009.
- [17] Wentao Li, Baoxiang Pan, Jiangjiang Xia, and Qingyun Duan. Convolutional neural network-based statistical post-processing of ensemble precipitation forecasts. *Journal of Hydrology*, 605:127301, 2022.
- [18] Andrew C Lorenc. Analysis methods for numerical weather prediction. *Quarterly Journal of the Royal Meteorological Society*, 112(474):1177–1194, 1986.
- [19] Peter Lynch. Weather prediction by numerical process. *The Emergence of Numerical Weather Prediction*, 11:1–27, 2006.
- [20] UC Mohanty, Krishna K Osuri, Vijay Tallapragada, Frank D Marks, Sujata Pattanayak, M Mohapatra, LS Rathore, SG Gopalakrishnan, and Dev Niyogi. A great escape from the bay of bengal “super sapphire–phailin” tropical cyclone: a case of improved weather forecast and societal response for disaster mitigation. *Earth Interactions*, 19(17):1–11, 2015.
- [21] Eike H Müller and Robert Scheichl. Massively parallel solvers for elliptic partial differential equations in numerical weather and climate prediction. *Quarterly Journal of the Royal Meteorological Society*, 140(685):2608–2624, 2014.
- [22] Vaino Nurmi, Adriaan Perrels, Pertti Nurmi, Silas Michaelides, Spyros Athanasatos, and Matheos Papadakis. Economic value of weather forecasts on transportation—impacts of weather forecast quality developments to the economic effects of severe weather. *EWENT FP7 project*, 490, 2012.

- [23] Adam Paszke, Sam Gross, Francisco Massa, Adam Lerer, James Bradbury, Gregory Chanan, Trevor Killeen, Zeming Lin, Natalia Gimelshein, Luca Antiga, Alban Desmaison, Andreas Kopf, Edward Yang, Zachary DeVito, Martin Raison, Alykhan Tejani, Sasank Chilamkurthy, Benoit Steiner, Lu Fang, Junjie Bai, and Soumith Chintala. PyTorch: An imperative style, high-performance deep learning library. 2019.
- [24] Jaideep Pathak, Shashank Subramanian, Peter Harrington, Sanjeev Raja, Ashesh Chattopadhyay, Morteza Mardani, Thorsten Kurth, David Hall, Zongyi Li, Kamyar Azizzadenesheli, et al. Fourcastnet: A global data-driven high-resolution weather model using adaptive fourier neural operators. *arXiv preprint arXiv:2202.11214*, 2022.
- [25] D Patil, I Szunyogh, B Hunt, J Yorke, E Ott, and E Kalnay. Applications of chaotic dynamics to weather forecasting. In *AGU Fall Meeting Abstracts*, volume 2001, pages NG42A–0412, 2001.
- [26] Ting Peng, Xiefei Zhi, Yan Ji, Luying Ji, and Ye Tian. Prediction skill of extended range 2-m maximum air temperature probabilistic forecasts using machine learning post-processing methods. *Atmosphere*, 11(8):823, 2020.
- [27] Adrian E Raftery, Tilmann Gneiting, Fadoua Balabdaoui, and Michael Polakowski. Using bayesian model averaging to calibrate forecast ensembles. *Monthly weather review*, 133(5):1155–1174, 2005.
- [28] Stephan Rasp, Peter D Dueben, Sebastian Scher, Jonathan A Weyn, Soukayna Mouatadid, and Nils Thuerey. Weatherbench: a benchmark data set for data-driven weather forecasting. *Journal of Advances in Modeling Earth Systems*, 12(11):e2020MS002203, 2020.
- [29] Stephan Rasp and Sebastian Lerch. Neural networks for postprocessing ensemble weather forecasts. *Monthly Weather Review*, 146(11):3885–3900, 2018.
- [30] Stephan Rasp and Nils Thuerey. Data-driven medium-range weather prediction with a ResNet pretrained on climate simulations: A new model for WeatherBench. *Journal of Advances in Modeling Earth Systems*, 13(2), 2021.
- [31] Olaf Ronneberger, Philipp Fischer, and Thomas Brox. U-net: Convolutional networks for biomedical image segmentation. In *International Conference on Medical image computing and computer-assisted intervention*, pages 234–241. Springer, 2015.
- [32] Suranjana Saha, Shrinivas Moorthi, Hua-Lu Pan, Xingren Wu, Jiande Wang, Sudhir Nadiga, Patrick Tripp, Robert Kistler, John Woollen, David Behringer, et al. The ncep climate forecast system reanalysis. *Bulletin of the American Meteorological Society*, 91(8):1015–1058, 2010.
- [33] Sebastian Scher. Toward data-driven weather and climate forecasting: Approximating a simple general circulation model with deep learning. *Geophysical Research Letters*, 45(22):12–616, 2018.
- [34] Sebastian Scher and Gabriele Messori. Weather and climate forecasting with neural networks: using general circulation models (gcms) with different complexity as a study ground. *Geoscientific Model Development*, 12(7):2797–2809, 2019.
- [35] Zoltan Toth and Eugenia Kalnay. Ensemble forecasting at nmc: The generation of perturbations. *Bulletin of the american meteorological society*, 74(12):2317–2330, 1993.
- [36] Stéphane Vannitsem, John Bjørnar Bremnes, Jonathan Demaeyer, Gavin R Evans, Jonathan Flowerdew, Stephan Hemri, Sebastian Lerch, Nigel Roberts, Susanne Theis, Aitor Atencia, et al. Statistical postprocessing for weather forecasts: Review, challenges, and avenues in a big data world. *Bulletin of the American Meteorological Society*, 102(3):E681–E699, 2021.
- [37] F Vitart. Evolution of ECMWF sub-seasonal forecast skill scores. *Q.J.R. Meteorol. Soc.*, 140: 1889-1899, 2014.
- [38] F. Vitart, M. Alonso-Balmaseda, A. Benedetti, B. Balan-Sarajini, S. Tietsche, J. Yao, M. Janousek, G. Balsamo, M. Leutbecher, P. Bechtold, I. Polichtchouk, D. Richardson, T. Stockdale, and C. Roberts. Extended-range prediction. *ECMWF Technical Memorandum 854*, 58 pp, 2019.

- [39] Jonathan A Weyn, Dale R Durran, and Rich Caruana. Can machines learn to predict weather? using deep learning to predict gridded 500-hpa geopotential height from historical weather data. *Journal of Advances in Modeling Earth Systems*, 11(8):2680–2693, 2019.
- [40] D.S. Wilks, R.E. Pitt, and G.W. Fick. Modeling optimal alfalfa harvest scheduling using short-range weather forecasts. *Agricultural Systems*, 42(3):277–305, 1993.
- [41] D.S. Wilks and D.W. Wolfe. Optimal use and economic value of weather forecasts for lettuce irrigation in a humid climate. *Agricultural and Forest Meteorology*, 89(2):115–129, 1998.
- [42] Wei Yao, Zhigang Zeng, Cheng Lian, and Huiming Tang. Pixel-wise regression using u-net and its application on pansharpening. *Neurocomputing*, 312:364–371, 2018.
- [43] Michaël Zamo and Philippe Naveau. Estimation of the continuous ranked probability score with limited information and applications to ensemble weather forecasts. *Mathematical Geosciences*, 50(2):209–234, 2018.
- [44] Ervin Zsótér. Recent developments in extreme weather forecasting. *ECMWF newsletter*, 107(107):8–17, 2006.